Journal of Visualization, Vol. 5, No. 2 (2002) 121-128

Dominant Vortices in Impinging Jet Flows

Tesař,V.*† and Barker, J.*

* Department of Chemical and Process Engineering, The University of Sheffield, Mappin Street, S1 3JD, Sheffield, UK.

Received 9 July 2000.
Revised 21 September 2001.

***Abstract*:** A novel method of flow visualization by dye was used in conjunction with numerical solutions to investigate the formation stages of large stationary vortical motions located in the "trajectory bend" centers of impinging jet flows. The vortices dominate the flowfield and were found to have profound influence on the wall transport phenomena. Depending on the value of Reynolds number, four regimes were identified with different flow character.

***Keywords*:** impinging jets, vortices, visualization, numerical solutions.

1. Introduction

Impinging jet flows, both planar and axisymmetric, are often used to provide very high heat and/or mass transfer rate between a fluid and a wall (heating, drying, cooling, ... e.g. Martin, 1977). As shown schematically in Fig. 1, the jet of hot fluid, accelerated in a nozzle, is directed against the surface to be heated. The flow has to change its direction from perpendicular towards parallel to the surface and the streamlines undergo a rather sharp "bending". There are several not yet fully understood features of impinging flows. In particular, distribution of heat and/or mass transfer on the wall - especially for small relative nozzle heights below about $h/b = 3$ (defined in Fig. 1) - exhibits often (though not always) peculiar and not completely explained secondary off-axis maxima. Gardon and Cahit Akfirat (1962) attempted to explain them as a consequence of laminar/turbulent transition - a view still often held in literature. According to a different hypothesis of one of the present authors (Tesař, 1998b - based upon detailed anemometric investigations), the off-axis maxima should be the result of "*lifting*" convected turbulence due to action of standing coherent vortices forming the curvature centres of the "*bends*". These vortices were found by Popiel and Trass (1991) using smoke wire visualization and also detected as coherent structures by Tesař and Střílka (1997) using a novel detection method. They are called here "dominant vortices" since they strongly influence and even dominate the flowfield. In most applications the impinging jets are turbulent (turbulence is welcome to increase the convective transport intensity) and there are smaller scale vortical motions of stochastic character in the flow, mainly generated in the shear layers on jet edges and carried with the flow. The dominant vortices differ from them by being coherent, statistically stationary, and of larger size. In visualizations of planar cases they appear as a pair of "*eyes*" - while in axisymmetric cases they form a standing vortex ring. They influence the conditions at the wall by generating induced rotational motions that "lifts" the fluid trajectories (Tesař, 1998b). This effect on the wall transfer phenomena was recently ascertained by visualizations of Meola et al. (2000).

The dominant vortices are found even in laminar flows, where in the absence of the superimposed small scale turbulence they are easier to investigate. At low Reynolds numbers one may even observe their early formation stages, which is useful for a deeper understanding of their character. Important property of the dominant vortices, especially in laminar flow, is their "*permanence*": limited exchange of fluid with their surroundings.

---

† on leave fromČVUT Praha, Czech Republic

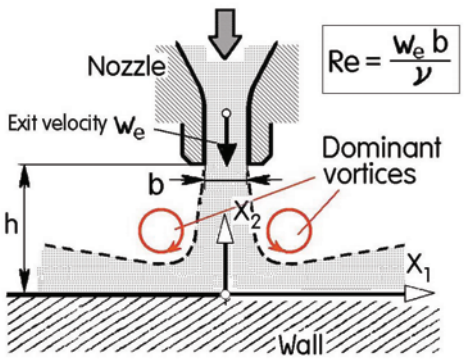

Fig.1. Schematic representation of an impinging jet, its main characterisation quantities and the two dominant vortex motions (shown in red).

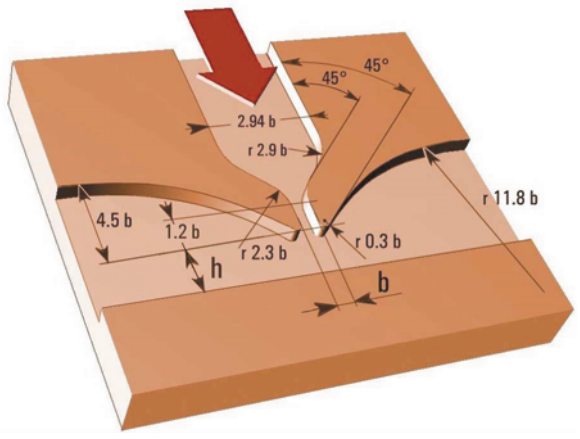

Fig. 2. The planar geometry: nozzle width b = 3.4 mm, relative height above the impingement wall h/b = 2.75.

2. Experiments

A flow visualization study backed by CFD flowfield solutions concentrated on the pair of the dominant vortices in a planar, nominally two-dimensional case at low Reynolds numbers. The geometry of the investigated flowfield domain is shown in detail in Fig. 2. The relative height of the nozzle above the wall h/b was in the range where wall heat transfer studies found the off-axial maxima ($h/b < 3$). For ease of visualization as well as keeping two-dimensionality, the spanwise distance between the end plates was small, only $0.41b$. The particular nozzle shape, with rounded exit lips, was taken over from a low Reynolds number application (Tesař 2001; Tesař et al., 2001). The geometry may be described as "*semi-confined*", with the nozzle exit inside a blended, wide and short projection. This places it between the "open" case, with nozzle exit at an end of a long (tubular) projection, and the "*confined*" case with the nozzle exit flush with a wall parallel to the impingement surface.

The working fluid was water. The visualization was by time-dependent dye concentration. Prior to each experiment, limited amount of dyed water (using powerful *Victoria blue* dye) was inserted into the supply pipe upstream from the nozzle. The dyed column was preceded and followed by clear water. On starting the run, only this clear water came into the nozzle. The dyed column reached the nozzle after a completely steady state was achieved. Majority of fluid in the camera field of view then underwent a change from transparent to dyed state. The permanence of the dominant vortices made possible to see them as regions of fluid remaining transparent in the dyed surroundings. Diffusion of the dyed water nevertheless took gradually place and the apparent size of the vortices decreased. As the dyed column passed through, the inverse change occurred: the surrounding water became transparent and the dominant vortices became visible as dyed regions. Flow velocities remained constant during these coloration changes.

There were several reasons for focusing the attention of the present study on the low Reynolds numbers (computed here from the nozzle exit maximum velocity and nozzle exit width, Fig. 1) between 200 and 1 500. One of them is that the formation stages of the vortices may provide clues for understanding their character. Other reasons were practical: ease of detection without turbulent unsteadiness and turbulent transport (higher permanence). Also the numerical computations there are most reliable, without limitations and uncertainty brought about by the various models of turbulence.

3. Computations

Standard FLUENT 5.4 commercial flow solver was used, its reliability validated earlier (Tesař, 2001) in flows of similar geometry and size. Full 3D formulation was used. The equations solved were those of laminar steady flow - so that rotation of vortices was recognisable only from closed patterns of pathlines. Assuming symmetry, only one half of the flowfield was actually computed to save computer time. The discretization used an unstructured

tetrahedral grid, made by first selecting particularly fine distribution of the nodes on the walls near the nozzle exit and stagnation point at the impingement wall, where the velocity gradients are highest and best spatial resolution necessary. Then the automatic grid generation of GAMBIT pre-processing software was used to build the rest by the "*paving*" method. The advantage of the unstructured grid is the possibility of adaption: in the present case the grid was adapted in the course of computations by addition of smaller elements in areas of high gradients of absolute velocity magnitude. Typically, the number of finite volume elements of the grid after adaption was in the range 50 000 - 60 000. Boundary conditions were constant velocity prescribed at the inlet upstream from the nozzle and constant pressure at the flow exit.

4. Results

At extremely small Reynolds numbers, in the creeping flow regime - which, of course, is outside the interest of applications - the dominant vortices are not formed. In fact, no jet forms, fluid propagating from the nozzle exit equally in all available directions. When Reynolds number is increased and jet directed in the nozzle axis direction is formed, more pronounced direction change takes place at the "*bending*" locations. Above $Re = 500$ the increased rotation velocity in the "*bend*" and higher relative effect of inertia causes vortical motions to appear. The dominant vortices are small at first, but their intensity as well as the size of domains surrounding them increases with *Re*. The surrounding recirculation domains gradually become elongated in the direction parallel to the wall as *Re* grows further. Finally, the flow along the wall acquires a character of a thin wall jet, with a distinct recirculation region above it. Above about $Re = 1\,500$, the flow ceases to be purely laminar. The dominant vortices are still detectable, but it is less easy to visualize them by the method used here due to turbulent mass transport reducing their permanence.

4.1 No Vortices in the Creeping Flow, Re < 300

In the particular example of such a flow (Fig. 3), the distribution of the dye in supply was uneven. This we usually strove to avoid, but here the generated streaks are useful providing an idea about shapes of streamlines. This may be made more apparent by replacing the continuous color density distribution by a posterizing discretization, an example of which is shown in Fig. 4. Isophots (lines of equal color density) are computed to divide the flowfield into areas. These are filled for easier recognition by different constant hue colors. The colors in the example Fig. 4 are false ones.

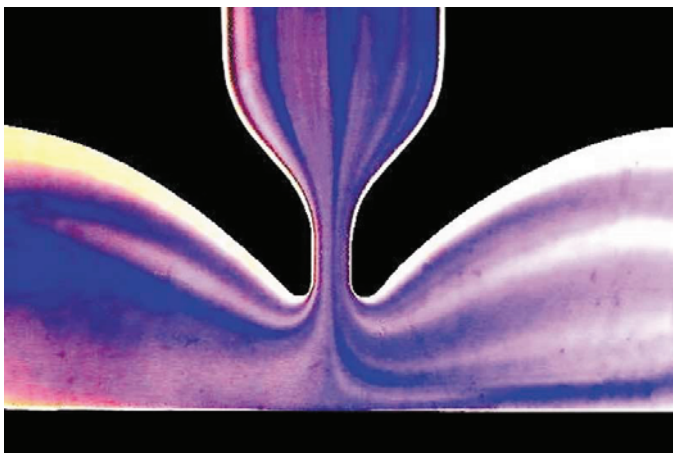

Fig. 3. Flow visualization photograph of the impinging flow at a very low Reynolds number $Re = 21$. In this subdynamic flow no dominant vortices are formed.

Instead of forming a jet, fluid tends here to move sideways immediately upon leaving the nozzle. The "*bend*" (the directional change) coincides with the rounded lip of the nozzle. The same conclusion is arrived at in the numerical solutions, (Fig. 5). The computed distribution of flow velocity in Fig. 6 is typical for these subdynamic flows. Although accelerated inside the nozzle, the fluid loses its velocity immediately downstream from the nozzle exit.

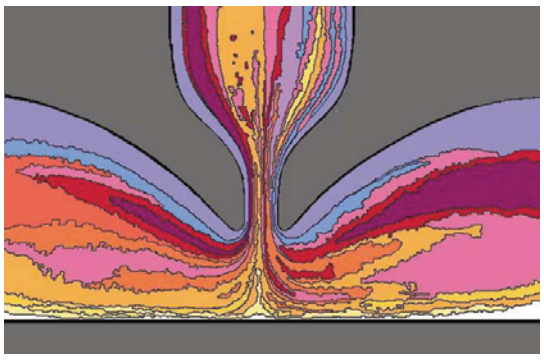

Fig. 4. Example of processing the visualization results: False colour rendering of Fig. 3 and posterization: continuous colour density field replaced by a stepwise distribution into discrete regions, each filled by a different (false) colour.

Another point of interest is the well visible existence of the stagnant insulation layers held at the walls by viscous effects. Making such layers well visible is a particular advantage of the present time-dependent dyeing flow visualization method. The dyed supply flow makes it possible to discern in Fig. 3 the bright regions at the walls in which the original transparent (low dye concentration) fluid still remains. Such bright areas, as could be expected, are seen in the boundary layers on nozzle walls in the top part of Fig. 3. Of particular importance for the impinging jets is the similar, thinner yet clearly recognizable bright layer on the impingement surface below. Heat and/or mass must get across this stagnant layer by conduction, much less effective than convection. This is why this layer, however thin, represents the main resistance in the transport phenomena between the fluid and the surface. A similar but less clearly recognizable resistance layer exists also in higher *Re* flows.

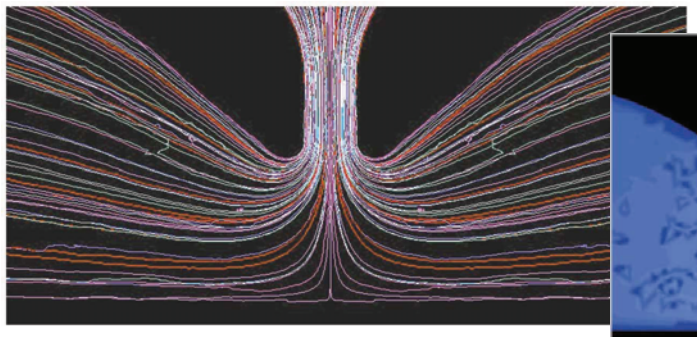

Fig. 5. A numerical solution of the subdynamic range flow. Pathlines of imaginary particles inserted in the nozzle. Although at a higher *Re* = 46, qualitative character of the flowfield corresponds to the experimental results in Figs. 3 and 4.

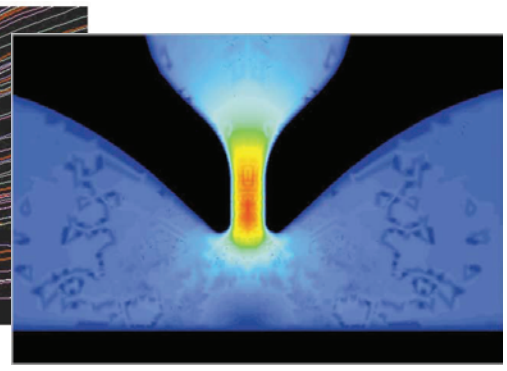

Fig. 6. Another example of subdynamic impinging flow: computed velocity magnitude at *Re* = 46, increasing from low values in blue areas to high values shown in red. Note the rapid loss of velocity downstream of the nozzle exit.

4.2 Embryonic Stage in the Transitional Regime 300 < Re <400

The dominant vortices do not appear immediately if the flow rate is increased beyond the limits of the subdynamic range. There is a transitional region - as documented by the flow visualization photograph taken in this region at *Re* around 350 in Fig. 7. The exact limits of this region are difficult to evaluate, 300 < *Re* <400 may be a rough guide. If velocity is increased so that Reynolds number becomes higher than the lower limit (*Re* ≈ 300), jet formation becomes evident. Very small regions of persistent fluid are seen to form directly at the nozzle exit lips, but below *Re* ≈ 400 there is no sign of their rotation - no dominant vortex pair is formed and despite the strong turning of the streamlines at both jet sides, the flow remains attached to the external nozzle wall.

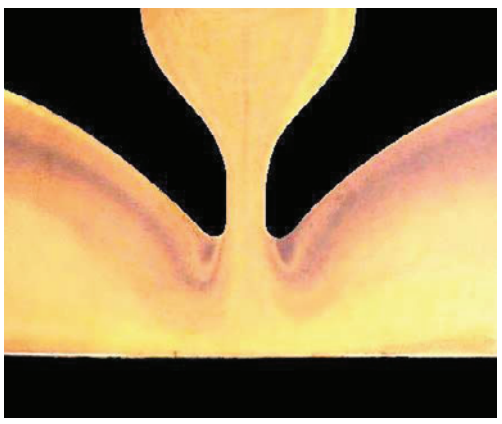

Fig. 7. Experiment: flow visualization at *Re* = 356 shows only vestigial patterns at the nozzle lips caused by the strong direction changes ("*bends*") on both sides of the jet - but no "dominant vortices".

4.3 Dominant Vortices in Laminar Flow, 400 < Re < 1 500

In this region, motion of various dirt particles present in the dominant vortices clearly show them to rotate in experiments or their video records. An example of computed pathlines just above the limit *Re*, (Fig. 8) reveals them by the closed pathlines at nozzle lips. A typical example of a flow visualization in this region, at *Re* = 568, is shown in Fig. 9. Later stages of the visualization procedure at the same conditions are in Figs. 10 and 11. The false color processing of Fig. 9 is shown in Fig. 12. Apart from the dye density distribution in the vicinity of the dominant vortices, indicating the extent and shape of the vortex regions, this processed picture shows the effect of "*lifting*" the flow above the wall as the flow proceeds past the vortex. This provides a support to the induced motion hypothesis discussed in Tesař, (1998b).

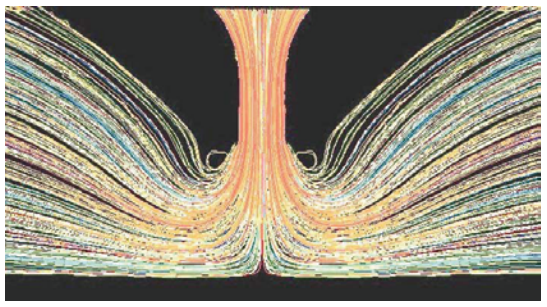

Fig. 8. Pathlines computed for the impinging flow at *Re* = 410, just above the lower limit for the existence of dominant vortices, which are seen here in their nascent stage.

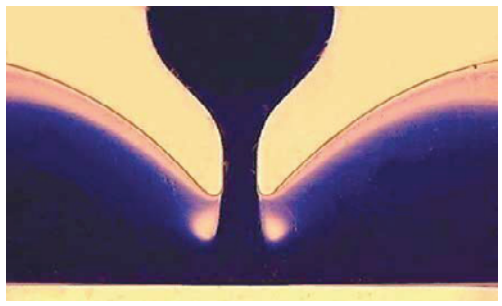

Fig. 9. The characteristic persistence of dominant vortices makes it possible to see them at *Re* = 568 as the "*pair of eyes*" - two regions retaining the original transparent fluid when concentration of dye in the supplied jet fluid is increased.

The dominant vortices were also identified in the numerical solutions. An example of the computed velocity field in Fig. 8 was evaluated for conditions in which the extent of vortical motion is very small and the vortices are still very close to the nozzle lips. In Fig. 10 there is another case with vortex cores further away. Representative case for this region is the case in Fig. 13. Numerical solutions make possible evaluation of quantities difficult to measure experimentally - such as vorticity, which is commonly used to define coherent vortices and the left side of Fig. 13 presents the distribution of vorticity (from blue: low values, through to red: high values). The comparison with pathlines shows the limitations of vorticity as means for identifying the dominant vortices. Despite its name, vorticity is far from synonymous with presence of rotation in fluid. Its level is high in what is essentially parallel flow in shear layers (see the high value in the boundary layers inside the nozzles in Fig. 13) while it may be zero in globally rotating flow, an elementary example being conditions in the potential vortex flow (apart, of course, from

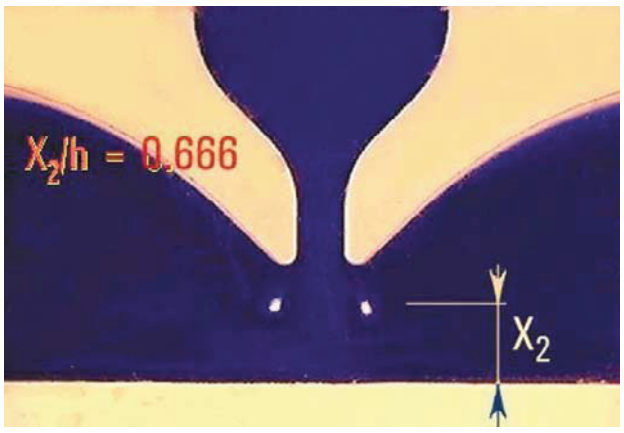

Fig.10. Photograph of the same flow as in Fig. 9 taken later when only vortex cores remain transparent. Note the persistence: in spite of dye diffusion, the vortices are still recognisable after elapsed time as long as $\Delta t = 625 b/w_e$.

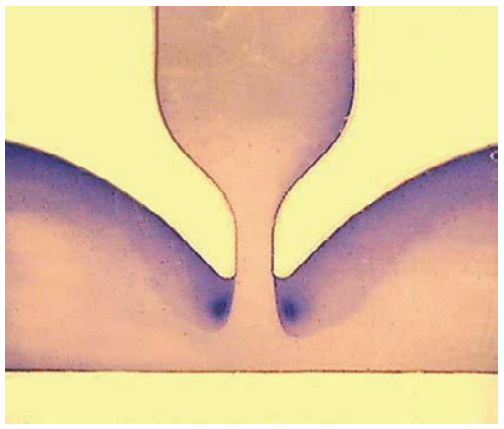

Fig.11. Photograph of the flow from Fig. 9 taken at still later time, $\Delta t = 1570\ b/w_e$ after dye entering the nozzle exit. There is no more dye in the supplied jet fluid. The dominant vortices are still there, made visible by their retention of the dyed fluid.

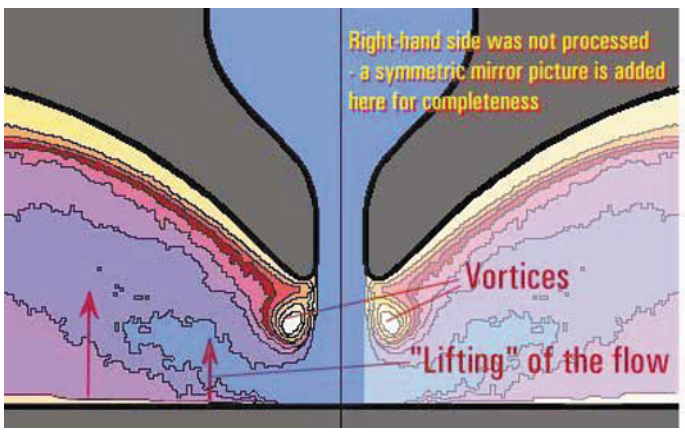

Fig.12. The false colour discretised (posterized) rendering of (left half of) Fig. 9.

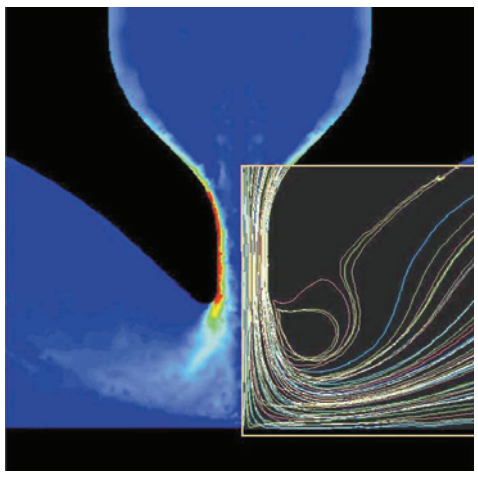

Fig.13. Computed vorticity distribution in the impinging jet flow at *Re* = 865 (left-hand side), compared with the extent of the rotating region surrounding the dominant vortex as revealed by pathlines.

its origin). In the present case, most of the dominant vortex region identified by persistence visualizations and computed pathlines exhibits essentially zero vorticity, while there is a strong vorticity in the mixing layers on jet edges.

It is important to discriminate between the dominant vortex recirculation region, identifiable due to its closed pathlines and containing the same fluid (- the reason behind its persistence) and the core in which the rotational motion inducing is concentrated. The two are shown in the example Fig. 14. The core is located rather eccentrically relative to the recirculation region boundaries. The present visualization method is particularly suitable to reveal the core location in the latest phases of the color change, as shown in Fig. 10. These locations are in very good agreement with computational results. The "lifting" effect of the dominant vortices on jet fluid trajectories (the motion away from the wall faster than what may be explained by the shear layer growth) is due to the trajectories curvature when flowing past the region boundary. Figure 15 shows the development of the

boundaries with increasing *Re*. Initially it forms at the nozzle lip. Then as *Re* grows, the decrease in effective viscous loss of jet momentum moves the boundary towards the impinging wall. At later stages, the region starts expanding transversely, in the direction along the impinging wall. This, however, only increases the eccentricity: the core remains located inside the "*bend*".

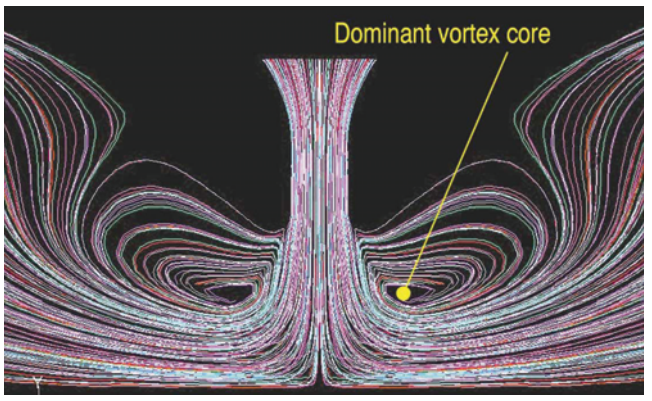

Fig.14. Pathlines computed for the impinging flow at *Re* = 1350, near the limit at which it becomes influenced by turbulence.

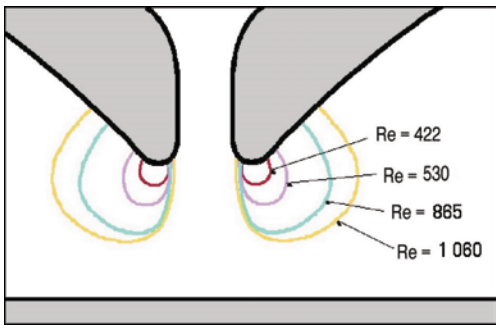

Fig.15. Variations with Reynolds number of the extent of the circulatory motion region.

4.4. Dominant Vortices in Turbulent Flow, Re > 1 500

In this regime, computations are less reliable due to intricacies of the low *Re* turbulence modeling and visualization becomes less reliable due to turbulent mixing of the dye. Again, the *Re* limit as stated above is only very approximate. Figure 16 shows an example still in the transition phase. Recirculation domain may extend effectively to infinity - and yet its core, the actual "dominant vortex", may be found even nearer to the axis, as the jet became narrower. The intensity of the core rotation is evident from the very sharp "*bending*" of the trajectories there.

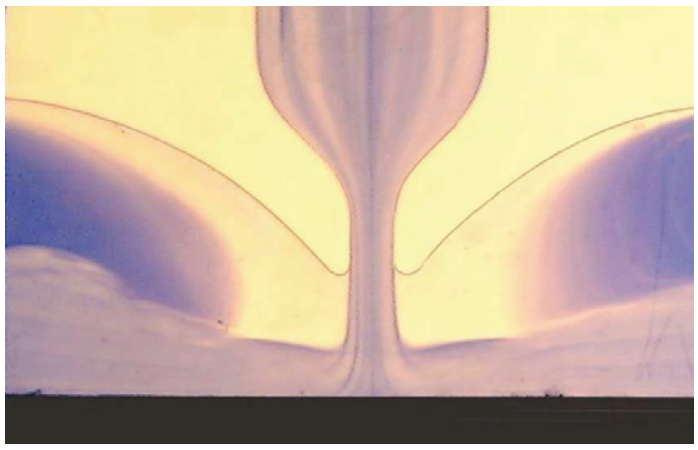

Fig.16. Flow visualisation at *Re* = 1 780. In the wall-jet parts the flow already became turbulent.

5. Conclusions

The authors used a novel visualization method which may be described as persistence method or time-dependent dyeing. If it was ever used before (no reference was found), they have invented it independently. It is suitable for the rather special situation of visualizing highly permanent flow features - such as the standing dominant vortices in the present case, especially in laminar flow. The essential result is finding the locations of the vortical domain boundaries as well as its core. For this the method is eminently suitable, in particular for core location the final

stages of the coloration change (Fig. 10). The relation between the highly eccentrically located core and the surrounding recirculation domain was clarified by following their development with increasing *Re*. The results are in good agreement with numerical solutions. Qualitatively, the features in the present "*semi-confined*" case may be applicable also to the "*confined*" cases.

References

Gardon, R. and Cahit Akfirat, J., The Role of Turbulence between a Flat Plate and Jets of Air Impinging on it, Proc. of 2nd Heat Transf. Conf., New York, (1962).

Martin, H., Heat and Mass Transfer between Impinging Gas Jets and Solid Surfaces, Advances in Heat Transfer, 13, Academic Press, New York, (1977), pp.1-60

Meola, C., Cardone, G., Carmicio, C., and Carlomagno, G. M., Fluid Dynamics and Heat Transfer in an Impinging Air Jet, Proc. of 9th Intern. Symp. on Flow Visualization, Edinburgh, (2000).

Popiel, C.O. and Trass, O., Visualization of a Free and Impinging Round Jet, Thermal Fluid Science, 4 (1991), pp.253.

Tesař, V. and Střílka, T., Koherentní struktura v ohybové partii axiálné excitovaného impaktního proudní (Coherent structure in the bending region of an axially excited impinging flow - in Czech), Proc. of Colloq. "Fluid Dynamics '97", ISBN 80-85918-28-3,/ÚAV R, Praha, Czech Republic, (1997).

Tesař, V., Excited Axisymmetric Impinging Flows, Proc. of Conf. "Engineering Mechanics '98", Volume 4, ISBN 80-85918-40-4, Svratka , Czech Republic, (1998), pp. 757-762.

Tesař, V., The Problem of Off-Axis Transfer-Effect Extremes in Impinging Jets, Proc. of XVIIth Intern. Conf. of Fluid Mechanics and Thermodynamics, ISBN 80-88896-19-3, Herlany, Slovakia, (1998), pp. 187-192.

Tesař, V., Low, Y. Y., Allen, R. W. K. and Tippetts, J. R, MICROFLUIDICS FOR MEMS - Microfluidic Valve, Proc. of PICAST IV Pacific Intern. Conf. on Aerospace Science and Technology, Kaoshiung, Taiwan, (2001), pp.301.

Tesař, V., Microfluidic Valves for Flow Control at Low Reynolds Numbers, Journal of Visualization, 4-1 (2001), pp.51-60.

Author Profile

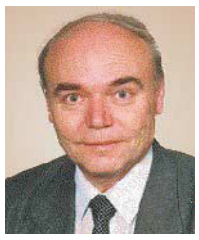

Václav Tesař: He received his Ing. degree in Mechanical Engineering in 1963 from ČVUT - Czech Technical University, Praha, Czech Republic. From 1963 to 1999 he was employed at ČVUT Praha as Assistant, later Docent and finally Full Professor. He recived C.Sc. degree (an equivalent of PhD) from ČVUT Praha in 1972. In 1985, he became Visiting Professor at Keio University, Yokohama, Japan. In 1992 he became Visiting Professor at Northern Illinois University, DeKalb, USA. From 1994 to 1998, he was Head of the Department of Fluid Mechanics and Thermodynamics, ČVUT Praha. He is currently Visiting Professor at the Department of Chemical and Process Engineering, The University of Sheffield, United Kingdom. His research interests are in shear flows, in particular jets and wall jets and their applications to fluidic no-moving-part flow control (named as inventor on 195 Czech Patents, mainly on fluidic devices, and on four British Patent Applications on microfluidic devices).

Jonathan Barker: He received his MSc degree in Chemical and Process Engineering in 2000 from The University of Sheffield, where during his final year he collaborated with Professor Tesař on investigations of impinging jet flows. He currently teaches English in Ika-gun, Shiga, Japan.